Neurobiology of Stress 33 (2024) 100676

Contents lists available at ScienceDirect

Neurobiology of Stress

journal homepage: www.elsevier.com/locate/ynstr

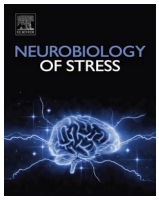

Dynamic changes of media prefrontal cortex astrocytic activity in response to negative stimuli in male mice

Ai-Mei Wu [a,b], Jing-Ya Zhang [a], Wei-Zhong Lun [a], Zhi Geng [c], Ye Yang [c], Jun-Cang Wu [b,**], Gui-Hai Chen [a,*]

[a] Department of Neurology (Sleep Disorders), The Affiliated Chaohu Hospital of Anhui Medical University, Hefei, Anhui, 230011, China
[b] Department of Neurology, The Second People's Hospital of Hefei, Hefei Hospital Affiliated to Anhui Medical University, Hefei, Anhui, 230011, China
[c] Department of Neurology, The First Affiliated Hospital of Anhui Medical University, Hefei, Anhui, 230011, China

ARTICLE INFO

Handling Editor: Dr. John Cryan

Keywords:
Astrocyte
Calcium activity
Media prefrontal cortex
Stress

ABSTRACT

Astrocytes play significant roles in regulating the central stress response. Chronic stress impairs the structure and function of astrocytes in many brain regions such as media prefrontal cortex (mPFC) in multiple neuropsychiatric conditions, but the astrocytic dynamics on the timescale of behavior remains unclear. Here, we recorded mPFC astrocytic activity in freely behaving mice and found that astrocytes are activated immediately by different aversive stimuli. Astrocyte specific GCaMP6s calcium indicator were virally expressed in mPFC astrocytes and fiber photometry experiments revealed that astrocytes are activated by tail-restraint (TRT), foot shock (FS), open arm exploration, stressor of height, predator odor and social defeat (SD) stress. ΔF/F analyses demonstrated that an unpredictable stimulus such as elevated platform stress (EPS) at the initial encounter induced the most intense and rapid changes in astrocytic calcium activity, while a predictable 2,5-dihydro-2,4,5-trimethylthiazoline (TMT) stimulus resulted in the weakest response with a longer peak latency. In TRT, FS or SD test, a somatic stimulus led to higher average calcium activity level and faster average peak latency in repeated trails. Similar to TMT stimulus, astrocytic calcium activity in elevated plus maze (EPM) test exhibited a smaller average change in amplitude and the longest peak latency during open arm exploration. Moreover, astrocytic calcium activity exhibited different changes across behavioral states in SD tests. Our findings show that mPFC astrocytes exhibit distinct patterns of calcium activity in response to various negative stimuli, indicating that the dynamic activity of astrocytes may reflect the stress-related behavioral state under different stimulus conditions.

1. Introduction

Astrocytes play multiple roles in regulating neuronal activity, synaptic plasticity, blood flow and behaviors (Kofuji and Araque, 2021; Sofroniew and Vinters, 2010; Volterra and Meldolesi, 2005). In response to stress or pathological conditions, astrocytes would undergo molecular, morphological, and functional changes (Aten et al., 2023; Bender et al., 2016; Cathomas et al., 2022; Murphy-Royal et al., 2019). Astrocytes working in coordination with neurons are emerging as key regulators of animal behaviors (Barnett et al., 2023; Kofuji and Araque, 2021) and the calcium signaling is considered to be the main mode of astrocyte communication (Bazargani and Attwell, 2016; Semyanov et al., 2020). In recent years, multiple studies have shown that the activation or attenuation of calcium signaling in astrocytes can impact neuronal synapse activity and complex behaviors, such as learning and memory, decision-making, fear conditioning, dominance behavior, as well as anxiety-like and depressive-like behaviors (Kofuji and Araque, 2021; Lu et al., 2022; Nagai et al., 2021; Noh et al., 2023; Yan and Liu, 2024). However, the dynamics and distinctions of calcium activity in astrocytes in response to different stressors remain unclear.

The medial prefrontal cortex (mPFC) plays critical roles in emotion processing, and its astrocytes are closely linked to stress response (Bender et al., 2016; Cathomas et al., 2022; Murphy-Royal et al., 2019). Modulating gene expressions in mPFC astrocytes can influence anxiety-like or depression-like behaviors in animals (Guo et al., 2024; Lu et al., 2022; Yao et al., 2023). For example, recent studies have shown that astrocytic lactate dehydrogenase in dorsomedial prefrontal (dmPFC) regulates neuronal excitability and depression-like behavior in

* Corresponding author.
** Corresponding author.
E-mail addresses: wujuncang126@126.com (J.-C. Wu), doctorcgh@163.com (G.-H. Chen).

https://doi.org/10.1016/j.ynstr.2024.100676
Received 9 July 2024; Received in revised form 21 August 2024; Accepted 1 October 2024
Available online 4 October 2024

mice by regulating extracellular lactate levels (Yao et al., 2023). Knocking down the expression of N6-methyladenosine demethylase ALKBH5 in mPFC astrocytes can reduce the immobile time in forced swimming and improve the depression-like behavior caused by chronic stress in mice (Guo et al., 2024). Additionally, changes in gene expression are closely related to changes in astrocyte calcium activity. Chronic social defeat stress in rodents impaired Ca2+ responses and subsequent ATP (adenosine 5′-triphosphate) release in the PFC (Cao et al., 2013). Serotonin-selective reuptake inhibitor (SSRI) antidepressants increase Ca2+ signaling in PFC astrocytes (Schipke et al., 2011). Lu et al. report that glucocorticoid receptors in the mPFC affected astrocytic Ca2+ activity and dynamic ATP release in response to stress (Lu et al., 2022). These studies suggest that mPFC astrocyte activity is involved in the regulation of stress-related disorders and the astrocytic calcium activity may directly reflect the behavioral changes induced by stress.

To understand the response of mPFC astrocytes to acute environmental stress in awake, freely behaving animals, we used fiber photometry to measure the total fluorescence of GCaMP6s expressed in astrocytes. Calcium imaging experiments revealed that mPFC astrocytes are immediately activated by all aversive cues tested thus far. Furthermore, the temporal and intensity differences in calcium activity are found in the diverse sensory stimuli. Our findings suggest that the activity of mPFC astrocytes is sensitive to stressors, and the coping strategies employed by mice in response to different stressors result in distinct patterns of activation. The dynamic activity changes of mPFC astrocytes may offer new insights into understanding the astrocyte-mediated mechanisms of stress-related disorders.

2. Materials and methods

2.1. Animals

C57BL/6J male mice (6−8 weeks, SiPeiFu, China) were used in this study. The mice were housed 5 per cage, on a 12 h light/dark cycles (lights on at 8:00 a.m.) with standard rodent chow and tap water accessible *ad libitum*. All animal studies were approved and guided by the Animal Care and Use Committee (LLSC20160165) of the Anhui Medical University. All efforts were made to minimize animal suffering as well as to reduce the number of animals used. Six C57BL/6J mice were used for calcium imaging experiments, and male CD1(ICR) retired breeders (8 month age, SiPeiFu, China) were used as aggressors in the social defeat experiments.

2.2. Stereotaxic surgery

Mice were deeply anaesthetized using 5% isoflurane in oxygen-enriched air (O^2 Concentrator, RWD, Shenzhen, China) and then fixed into a stereotaxic frame (RWD Life Science, Shenzhen, China). Anaesthetized mice were maintained on 2–2.5% isoflurane, and a core body temperature was maintained at 36 °C using a feedback-controlled temperature controller (ATC2000, RWD Life Science, Shenzhen, China). Eye ointment was applied to prevent dryness. The head was shaved, and the skin was sterilized using iodine solution. Then, a midline incision was made with a scalpel to expose the skull.

AAV5-GfaABC1D-GCaMP6s virus (200 nl, 5.04×10^{12} genomic copies per ml, PT-2475, BrainVTA, China) was stereotaxically injected unilaterally into the mPFC using pulled glass pipettes (tip diameter 10–20 μm, PC-100 puller), connected to a pressure ejector (Micro4, WPI, USA). The mPFC coordinates used were: 1.7–1.8 mm anterior to bregma, ±0.3–0.4 mm lateral to the midline and 1.5–1.8 mm below the dura.

Mice were received unilateral implantation of an optical fiber (0.37 NA, 200 μm diameter, Inper Inc.) 2 weeks after viral vector injection. Optic fibre tips were lowered to 100–200 μm above the injection site. Fiber was secured to the skull using screws and dental cement.

2.3. Fiber photometry recording

Fiber photometry recording experiments were conducted 4 weeks after viral infections. To record fluorescent signals emitted by GCaMP, a fiber photometry system (ThinkerTech, Nanjing) was employed (Wang et al., 2024; Zhou et al., 2024). Briefly, laser beam generated by a 488 nm laser (OBIS 488LS; Coherent) was reflected by a dichroic mirror (MD498; Thorlabs) with a low-level power (20–40 μW) at the tip of optical fiber to minimize bleaching and kept constant during a recording session. The fluorescent signals were bandpass filtered, converted to voltage signals, digitalized at 100 Hz and then recorded using a custom-written script in LabView. Animals underwent fiber photometry recording were conducted in a tail-restraint test (TRT), elevated plus maze (EPM), elevated platform stress (EPS), 2,5-dihydro-2,4,5-trimethylthiazoline (TMT), pentyl acetate, sesame oil odor test, foot shock (FS) or social defeat (SD) task. Behavior-coupled fluorescent events were determined by peri-stimulus time histograms (PSTH) calculated as ΔF/F. Spontaneous calcium event analysis was performed for each photometric recording data to verify the effectiveness of the data. The signal from the 405 nm channel was used as control data to exclude motion noise and to verify the validity of the calcium signal channel data. MATLAB R2017b (MathWorks) was used for calcium fluorescence signal analyses, encompassing representative plotting, generation of average trace or heatmap graphs, and calculation of peak values of ΔF/F (%) and the matched time points. Post-mortem examination was utilized to confirm GCaMP expression and optical fiber placement.

2.4. Behavioral tasks

2.4.1. Tail-restraint test (TRT)

The tail of tested mice was chased and grabbed by hand. After grabbing, the mice were suspended in air for 30 s before releasing them in their home cage. Three repeated trails were performed with a 1 min interval. Calcium signals were recorded in homecage before tests and during TRT.

2.4.2. Elevated plus maze (EPM)

The maze consisted of a plus-shaped apparatus, with 2 opposite closed arms (30 cm × 6 cm) enclosed with walls (15 cm in height) and 2 opposite open arms (30 cm × 6 cm, without walls). The whole apparatus had a central arena (6 cm × 6 cm) and was elevated 80 cm above the floor. Each mouse was placed in the closed arena of the maze and allowed to explore the maze for 5–10 min. Calcium signals were recorded during the whole tests.

2.4.3. Elevated platform stress (EPS)

Mice were exposed to an established elevated platform standing behavioral paradigm (Zhang et al., 2020), which elicits acrophobia-related stress. Briefly, mice were individually placed on a transparent plastic platform of 10 cm in diameter and raised 150 cm above the ground. Calcium signals were recorded during homecage activity and on the platform for 3 min respectively. For each session, the animal was acoustically and visually isolated for the indicated amount of time.

2.4.4. Presentation of odorants

This task refers to previous research (Kim et al., 2019; Saraiva et al., 2016) and is slightly modified. Briefly, mice were habituated for 5min in a chamber box (30 cm × 30 cm × 30 cm). A piece of 2-cm^2 filter paper soaked with 50 μl of either water or pentyl acetate (1:10 diluted, Sigma Aldrich), sesame oil or 2,5-dihydro-2,4,5-trimethylthiazoline (1:10 diluted, Sigma Aldrich), was gently presented at the corner of the chamber. Calcium signals were recorded during habituation and odors presentation stages.

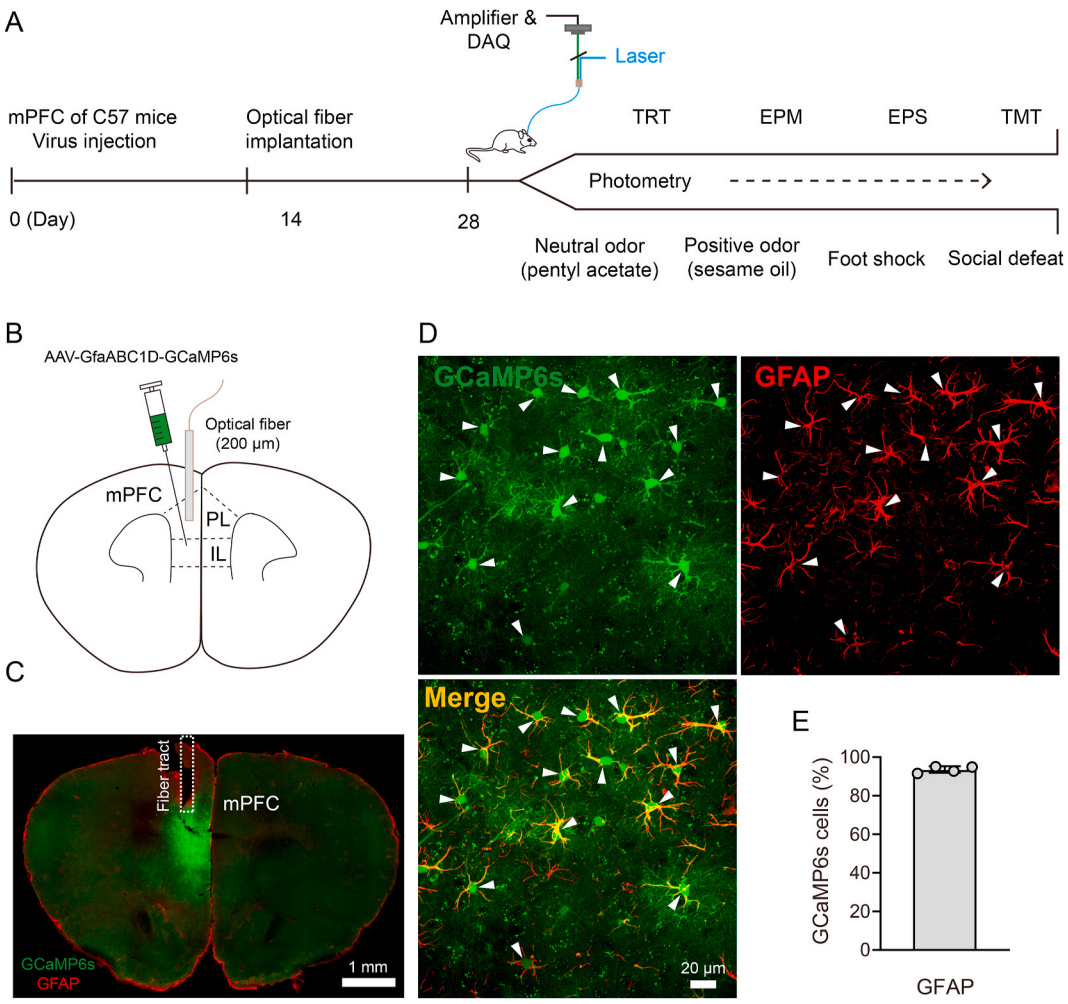

Fig. 1. Experimental timeline and strategy for recording mPFC astrocytic activity
A. Timeline of calcium indicator virus injection in mPFC astrocytes, fiber implantation and fiber photometry recording in mice under diverse stimuli. B. Viral injection and implantation scheme for fiber photometry on mPFC astrocytes. C. A representative image validates GCaMP6s expression in mPFC astrocytes and optical fiber tract above the injection site. D. Magnified images depict the overlap between GCaMP6s-expressing cells (green) and anti-GFAP-positive cells (red). E. Colocalization analysis of GCaMP6s positive cells and GFAP labeling (762 GCaMP6s positive cells from 12 slices, 4 mice).

2.4.5. Foot shock (FS)

Mice were habituated for 150 s in a shock chamber with a metal grid floor and transparent plastic walls, then a foot shock (0.5 mA, 2 s) was delivered and repeated three times (60 s inter-trial-interval). Calcium signals were recorded during habituation and shock stages.

2.4.6. Social defeat (SD)

Male CD1(ICR) retired breeders (8 month age, SiPeiFu, China) were screened for aggressive behaviors. An experimental mouse was habituated for 150 s in a separate space by a baffle in the home cage of a CD1 aggressor. During the exposure after the baffle was removed, the experimental mouse was physically defeated by the aggressor. Calcium signals were recorded during habituation and CD1 exposure stages.

2.5. Immunohistochemistry

Mice were transcardially perfused with ice-cold 0.1 M phosphate buffered saline (PBS; pH 7.4), followed by perfusion with ice-cold 4% paraformaldehyde in 0.1 M PBS. Whole brains were post-fixed in 4% paraformaldehyde in 0.1 M PBS overnight at 4 °C and cryoprotected with 30% sucrose. Coronal 40 μm thick sections were incubated in cryoprotectant at −20 °C until immunohistochemical staining was performed. The sections were incubated in a blocking solution containing 5% normal donkey serum (Jackson ImmunoResearch, Bar Harbor, ME, USA) and 0.1% Triton X-100 (Sigma-Aldrich) for 1 h at room temperature. Subsequently, the sections were incubated with mouse anti-GFAP (MAB360, 1:1000; Millipore) antibody overnight at 4 °C in the blocking solution. After washing with 0.1 M PBS, the sections were incubated for 2 h with Alexa Fluor 594-conjugated secondary antibodies (1:200, Jackson Immuno Research) in the blocking solution at room temperature, washed three times, and then mounted on glass slides using Vectashield mounting media with DAPI (Vector Laboratories, USA). Fluorescent images of the mounted sections were obtained using a confocal microscope (LSM880; Carl Zeiss, Germany).

2.6. Statistical analysis

Data were analyzed using GraphPad Prism software (version 9; San Diego, CA, USA). One-way ANOVA with Tukey's multiple comparisons test (ΔF/F analysis in different trails or stimuli) and unpaired *t*-test (ΔF/F analysis between water and TMT in odor tests) were performed. The apex point of the traced curve was defined as the peak value of ΔF/F (%). We considered p-value$<$0.05 as statistically significant. Data are expressed as group mean ± SEM (standard error of the mean) for each group.

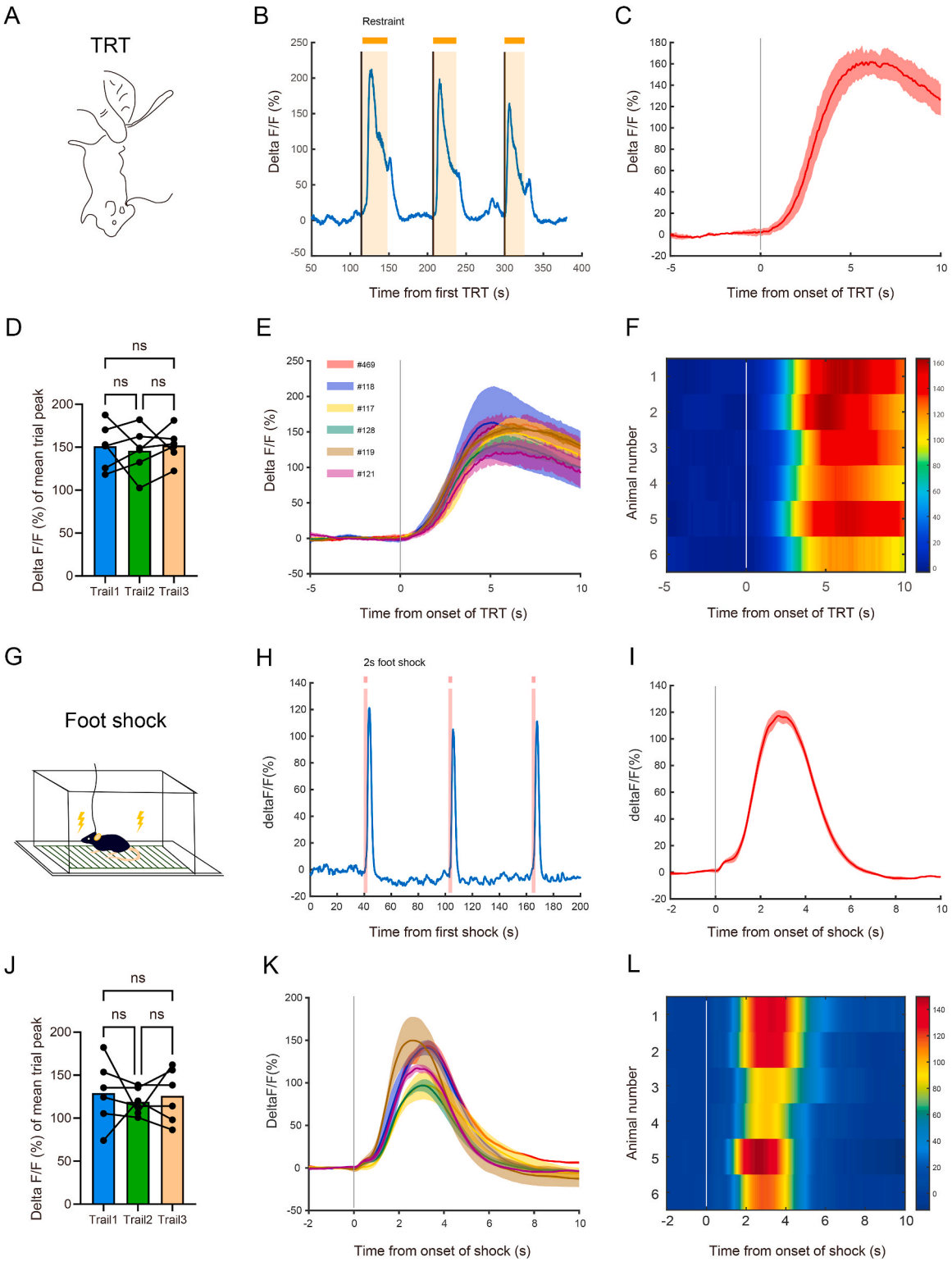

Fig. 2. Changes of astrocytic calcium signaling in the mPFC of mice subjected to TRT and foot shock

A. Schematic for TRT. B. A representative trace illustrating increases of mPFC astrocytic GCaMP6s signal during restraint (orange bars, above). Color-coded shaded bars depict the periods during which mice were chased by a hand (gray) and struggled (faint yellow). C. A representative peri-event plot of the mean Ca^{2+} transient during the repeated TRT in a mouse (n = 3 trails). The red line indicates the mean, and the shaded area indicates SEM. D. Statistical comparison of mean peak fluorescence signals in three trails during the repeated TRT. (n = 6 mice). E. The peri-event plot of the mean Ca^{2+} transient during the TRT in individual mouse (n = 6 mice). The colored lines indicate the mean, and the shaded area indicates SEM of individual mouse. F. Heat map of Ca^{2+} signals across animals aligned to the start of TRT (n = 6 mice). G. Schematic for foot shock. H. A representative trace illustrating increases of GCaMP6s signal during 2s shock (pink bars, above). Color-coded shaded bars depict the periods during which mice were under shocks. I. A representative peri-event plot of the mean Ca2+ transient during the repeated shock in a mouse (n = 3 trails). The red line indicates the mean, and the shaded area indicates SEM. J. Statistical comparison of mean peak fluorescence signals in three trails during the repeated shock. (n = 6 mice). K. The peri-event plot of the mean Ca^{2+} transient during the shock in individual mouse (n = 6 mice). The colored lines indicate the mean, and the shaded area indicates SEM of individual mouse. L. Heat map of Ca^{2+} signals across animals aligned to the start of shock (n = 6 mice).

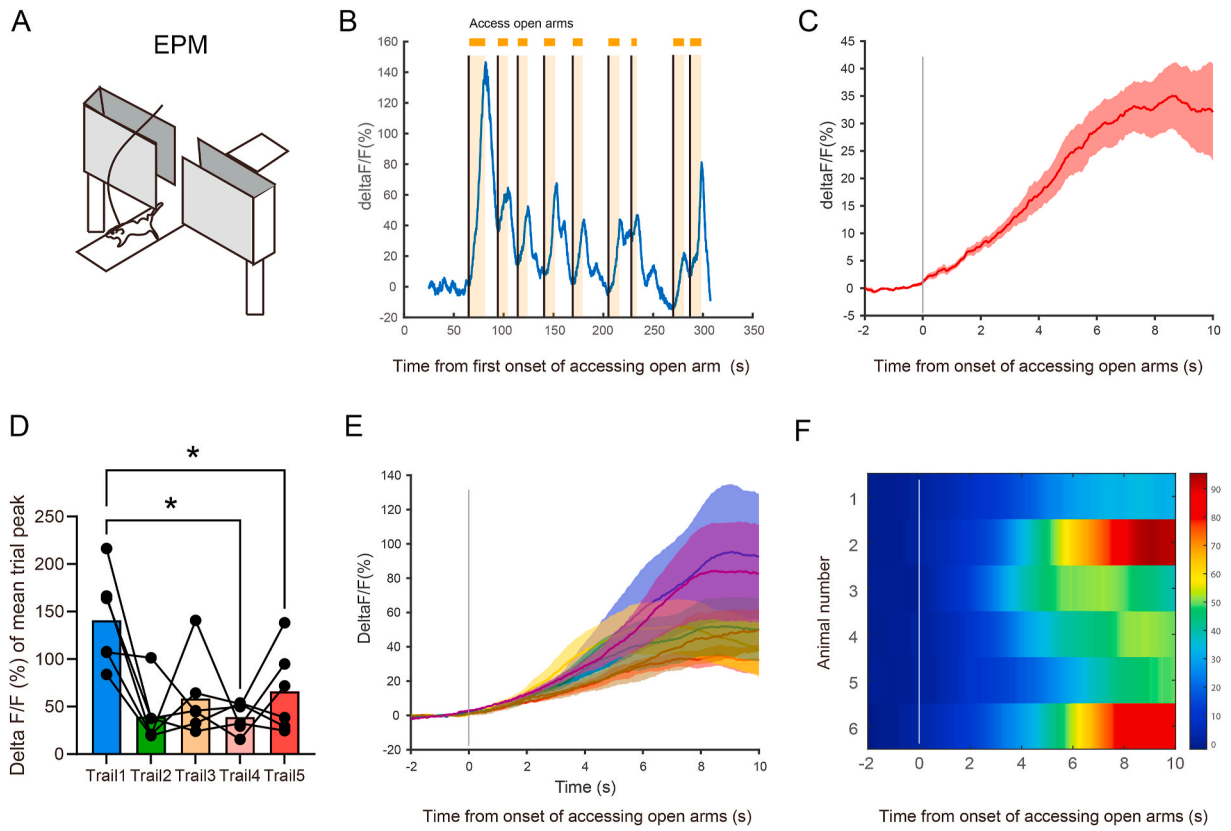

Fig. 3. Changes of mPFC astrocytic calcium signaling of mice exploring open arms in EPM
A. Schematic for EPM. B. A representative trace illustrating increases of mPFC astrocytic GCaMP6s signal during open arm explorations (orange bars, above). Color-coded shaded bars depict the periods during which mice approach (gray) and enter into (faint yellow) the open arms. C. A representative peri-event plot of the mean Ca^{2+} transient before and after entering into the open arms in a mouse. The red line indicates the mean, and the shaded area indicates SEM. D. Statistical comparison of mean peak fluorescence signals in five trails during open arm explorations (n = 6 mice). E. The peri-event plot of the mean Ca^{2+} transient during open arm explorations in individual mouse (n = 6 mice). The colored lines indicate the mean, and the shaded area indicates SEM of individual mouse. F. Heat map of Ca^{2+} signals across animals aligned to the start of open arm explorations (n = 6 mice).

3. Results

3.1. Experimental strategies for recording the activity of mPFC astrocytes in mice

To examine the changes in the activity of mouse mPFC astrocytes during diverse stimuli, we employed in vivo calcium imaging experiments by fiber photometry to record the changes of calcium signaling in mice subjected to TRT (tail-restraint test), EPM (elevated plus maze), EPS (elevated platform stress), aversive odor (TMT, 2,5-dihydro-2,4,5-trimethylthiazoline), neutral odor (pentyl acetate), positive odor (sesame oil), foot shock (FS) and social defeat (SD) conditions (Fig. 1A). We virally expressed a GFAP promoter-dependent GCaMP6s calcium indicator in C57BL/6J mice, and recorded changes in GCaMP6s fluorescence signal through a 200-μm optic fiber placed above the mPFC (Fig. 1B). The resulting trace represents the integrated activity of mPFC astrocytes. Histological analysis revealed that most of GCaMP6-expressing cells overlap with GFAP-positive cells (93.55% ± 1.703) in the mPFC in mice that were used for calcium imaging experiments (Fig. 1C–E).

3.2. Substantial and consistent increase in mPFC astrocytic activity by somatic stimuli

We investigated changes in GCaMP6 fluorescence intensity in mPFC-Astrocyte ^{GCaMP6} mice that were subjected to various stress-inducing conditions. During tail-restraint test (TRT), we observed a rapid increase in GCaMP intensity in mPFC astrocytes when mice were chased and lifted by hand (Fig. 2A–C). During three rounds of TRTs lasting 30 s each, the ΔF/F reached its peak at approximately 5 s (Fig. 2C and E) and then rapidly declined, returning to the baseline levels by the end of TRT (Fig. 2B). The peak ΔF/F in most mice gradually increased (Fig. 2B and D) but the average peak level of ΔF/F did not differ significantly across the three trails (Fig. 2D, one-way ANOVA, F(1.672, 8.360) = 0.1302, P = 0.8455). The ΔF/F curves of GCaMP fluorescence exhibited a consistent pattern among all the mice following TRT (Fig. 2E and F). In foot shock (FS) test (Fig. 2G), a 2-s shock also elicited a rapidly increasing calcium signal in the repeated trails (Fig. 2H). The ΔF/F reached its peak approximately 1 s after the shock ended, returning to the baseline at about 6 s from onset of the shocks (Fig. 2I). The mean peak levels in the three trails did not show significant differences (Fig. 2I, one-way ANOVA, F(1.310, 6.548) = 0.3422, P = 0.6358), and the pattern of calcium signal change after the foot shock was similar among different mice (Fig. 2K and L).

3.3. Increase in mPFC astrocytic activity during exploration of open arms in EPM

mPFC astrocytic activity also increased in mice when exploring open arms in EPM tests. The EPM consisted of a closed arm and an open arm, providing the mice with opportunities for spatial exploration and calcium imaging (Fig. 3A). GCaMP signals started to rise as the mice approached the open arm from the closed arm and reached their peak in the open arm, and began to decrease as they headed toward and entered into the closed arms again (Fig. 3B and Supplementary movie 1). The ΔF/F reached its peak at approximately 8–10 s (Fig. 3C and E), but the values depended on the duration of the mice's exploration in the open

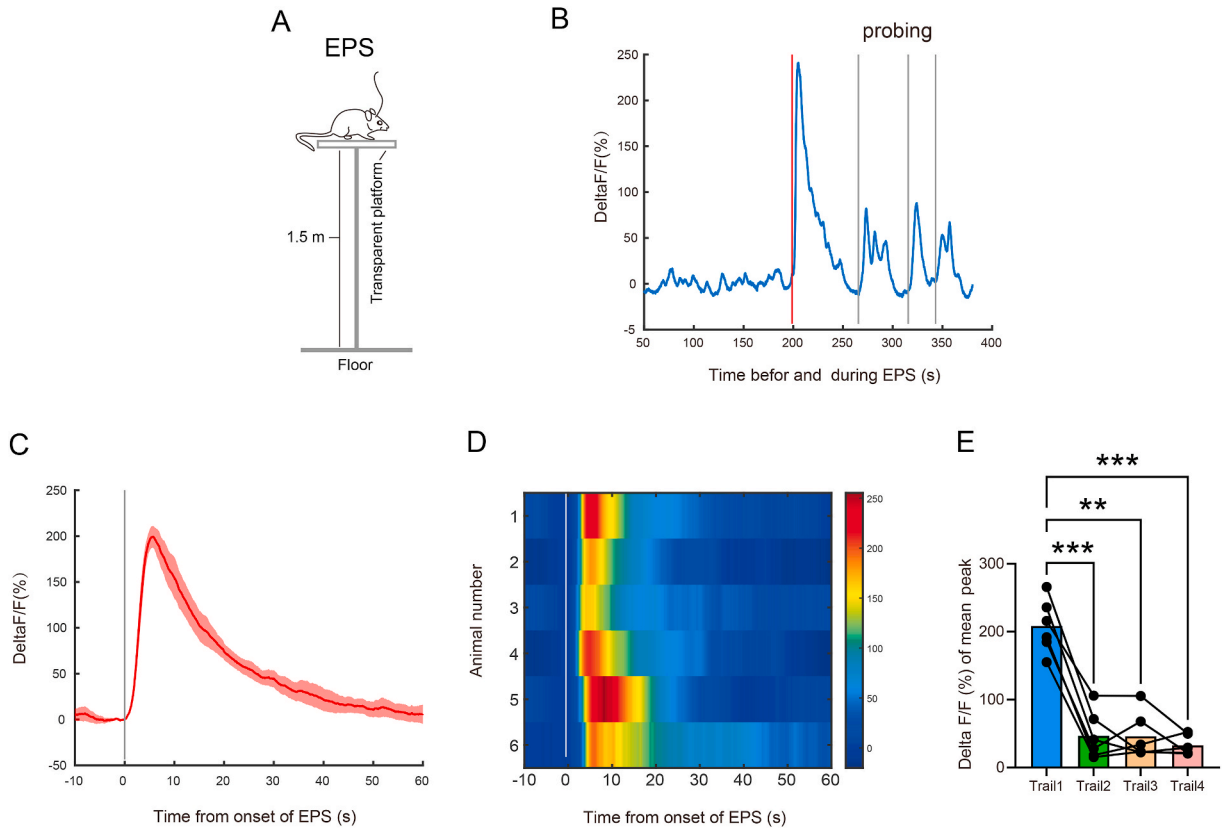

Fig. 4. Changes of astrocytic calcium signaling in the mPFC of mice subjected to EPS
A. Schematic for EPS. B. A representative trace illustrating increases of mPFC astrocytic GCaMP6s signal before and after EPS. Color lines represent the onset of increases in initial exploration (red) and subsequent probes (gray) on the platform. C. The peri-event plot of the mean Ca^{2+} transient before and after initial explorations of the platform (n = 6 mice). The red line indicates the mean, and the shaded area indicates SEM. D. Heat map of Ca^{2+} signals across animals aligned to the onset of EPS (n = 6 mice). E. Statistical comparison of mean peak fluorescence signals in four trails during platform explorations (n = 6 mice).

arm. However, the maximum value of the GCaMP signal is typically observed during the initial exploration (trail 1) of the open arms (Fig. 3B). The average peak of ΔF/F decreased significantly during the subsequent exploration of the open arm compared to the first trail (Fig. 3D, one-way ANOVA, F (3.183, 15.92) = 7.962, P = 0.0016). The average amplitude of GCaMP signals increased during exploration of the open arm varied among individual mice (Fig. 3E and F).

3.4. Increase in mPFC astrocytic activity in EPS test

During EPS, the mice were subjected to a sudden and persistent stressor of heights (Fig. 4A). This stimulus resulted in a substantial increase in GCaMP intensity and the strongest activation of mPFC astrocytes (Fig. 4B and C). The maximal GCaMP signal peaks occurred approximately 10 s post-stimulation, followed by a gradual return to the pre-EPS baseline level over a period of about 40 s (Fig. 4C). Notably, during continued exploration of the platform, there was a relatively small amount increase in GCaMP signals each time the mouse's head protruded from the platform (Fig. 4B). The changes of GCaMP intensity in different mice before and after the stimulus showed strong consistency, and the average peak of ΔF/F decreased significantly during the subsequent exploration on the platform compared to the first trail (Fig. 4E, one-way ANOVA, F (1.802, 9.010) = 56.89, P < 0.0001).

3.5. Different olfactory stimuli stimulate the activity of mPFC astrocytes

Next, we tested the effects of different types of olfactory stimuli (aversive odor TMT, neutral odor pentyl acetate, positive odor sesame oil) on calcium activity in mPFC astrocytes. Exposure to a predator odor, TMT, mostly triggered freezing responses in mice. We investigated changes in mPFC astrocytic activity by successively administering olfactory stimuli of water or TMT to mice (Fig. 5A). Initially, upon exposure to water, there was a moderate increase in calcium signals from mPFC astrocytes (Fig. 5B). However, after exposure to TMT, we observed a significant increase in the intensity (Fig. 5B–D) of GCaMP signals in astrocytes at the moment of TMT odor sniffing (Fig. 5B) by the mice, as compared to their response to water. The ΔF/F reached its peak at approximately 8 s (Fig. 5C). Furthermore, the mean peak ΔF/F of mice exposed to TMT during sniffing was significantly higher compared to that of water (Fig. 5E, paired *t*-test, t = 5.816, df = 5, P = 0.0021). After exposure to pentyl acetate (Fig. 5F), the ΔF/F mean peaks exhibited a slight increase in comparison to water exploration, with similar peak latency periods (Fig. 5G). Notably, the scent of sesame oil also elicited small increases in calcium signaling, but the magnitude and temporal pattern of this change were similar to those observed during water sniffing (Fig. 5G). There was no significant disparity in the mean peak calcium signal values across the three types of odor stimulation (Fig. 5H, one-way ANOVA, F (1.313, 6.563) = 1.392, P = 0.2943).

3.6. Changes in calcium activity of mPFC astrocytes under social defeat conditions

Upon exposure to CD1 mouse territory, test mice experienced aggressive encounters leading to flight or freezing responses. We conducted a comparative analysis of changes in mPFC astrocytic calcium activity across these behavioral responses (Fig. 6A and B). Specifically, prolonged CD1 attacks (lasting >3 s) consistently elicited robust peaks of calcium signaling (Fig. 6B and C, blue bars indicated, and D), whereas

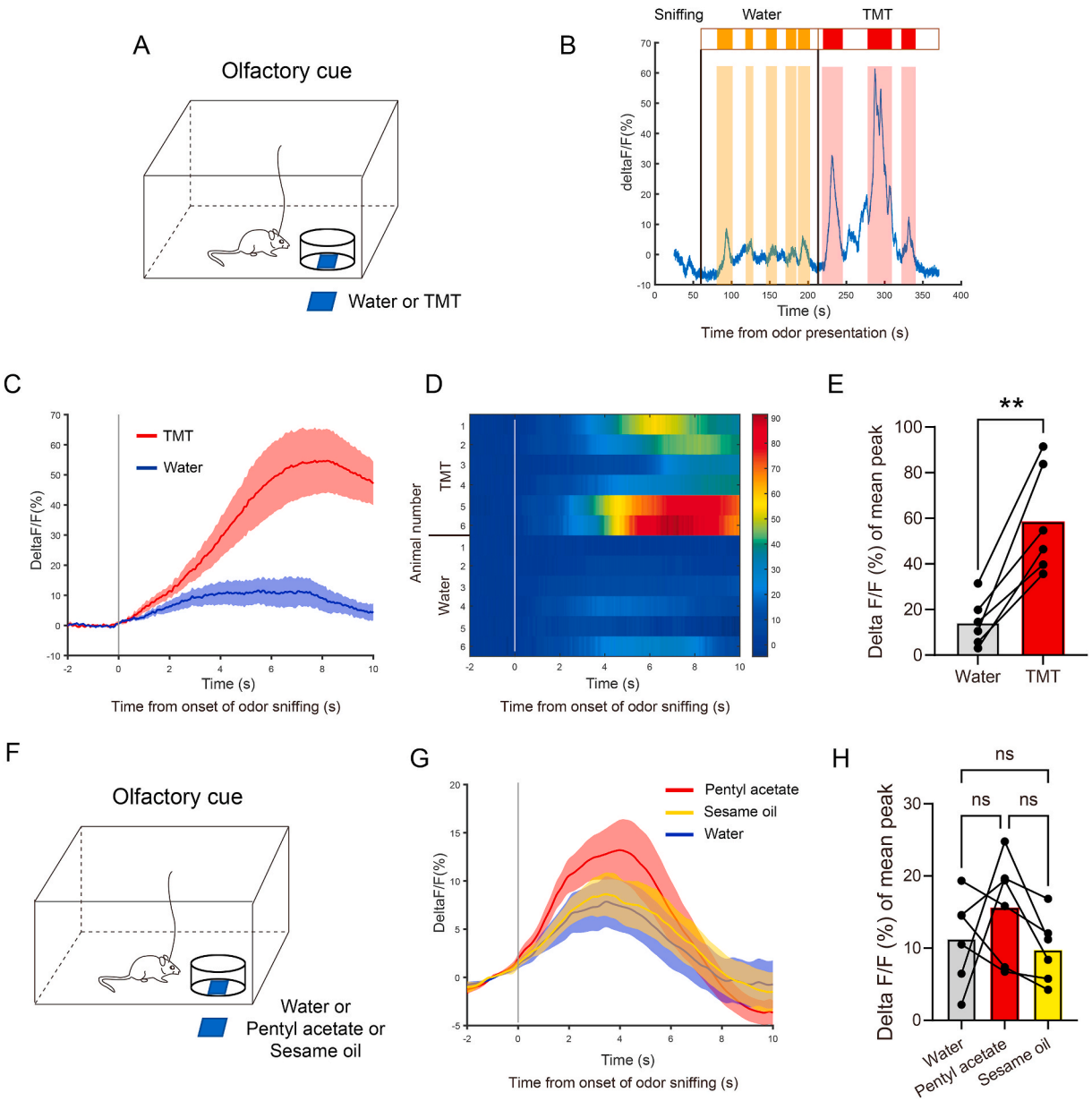

Fig. 5. Changes of astrocytic calcium signaling in the mPFC of mice subjected to olfactory stimuli
A. Schematic of odor (aversive) presentation. B. A representative trace showing increases of mPFC astrocytic GCaMP6s signal during water (orange bars, above) or TMT (red bars, above) exposure. Shaded bars depict the periods during which mice sniff water (faint yellow) or TMT (pink). C. The peri-event plots of the mean Ca^{2+} transient before and after odor sniffing of water and TMT (n = 6 mice). The blue line and the shaded area indicate the mean and SEM in water exposure, and the red line and the shaded area indicate the mean and SEM in TMT exposure. D. Heat map of Ca^{2+} signals across animals aligned to the period during odor sniffing of water and TMT (n = 6 mice). E. Comparison of mean peak GCaMP6s signals during water and TMT exploration sessions (n = 6 mice). F. Schematic of odor (neutral or positive) presentation. G. The peri-event plots of the mean Ca^{2+} transient before and after odor sniffing of water, pentyl acetate or sesame oil (n = 6 mice). The blue line and the shaded area indicate the mean and SEM in water exposure, the red line and the shaded area indicate the mean and SEM in pentyl acetate exposure, and the yellow line and the shaded area indicate the mean and SEM in sesame oil exposure. H. Comparison of mean peak GCaMP6s signals during water, pentyl acetate and sesame oil exploration sessions (n = 6 mice).

brief attacks resulted in modest increases (Fig. 6B and C, red bars indicated, and D). Furthermore, a slight elevation in calcium signaling levels was also elicited when test mice exhibited flight (Fig. 6B and C, yellow bars indicated, and D) or freezing (Fig. 6B and C, green bars indicated, and D) responses in the presence of approaching CD1 individuals Notably, aggression exceeding 3 s led to significantly higher increases in calcium signaling compared to the other observed behaviors (Fig. 6E, one-way ANOVA, $F(3, 60) = 55.94$, $P < 0.0001$). Shorter attack durations exhibited quicker peak latencies for calcium signals relative to other behaviors tested, however there was no significant difference in their average peak latency (Fig. 6F, one-way ANOVA, $F(3, 60) = 1.860$, $P = 0.1460$).

3.7. *The variances in calcium activity of mPFC astrocytes in response to diverse aversive stimuli*

We further conducted a comparative analysis of the differences in calcium activity of mPFC astrocytes induced by the various aversive stimuli, with a focus on the magnitude of fluorescence increase and the latency to peak fluorescence (Fig. 7). In the initial response to various stressors in mice (first TRT, first FS, first open arm exploration, sudden EPS, first TMT odor exploration and first attack), calcium signals of

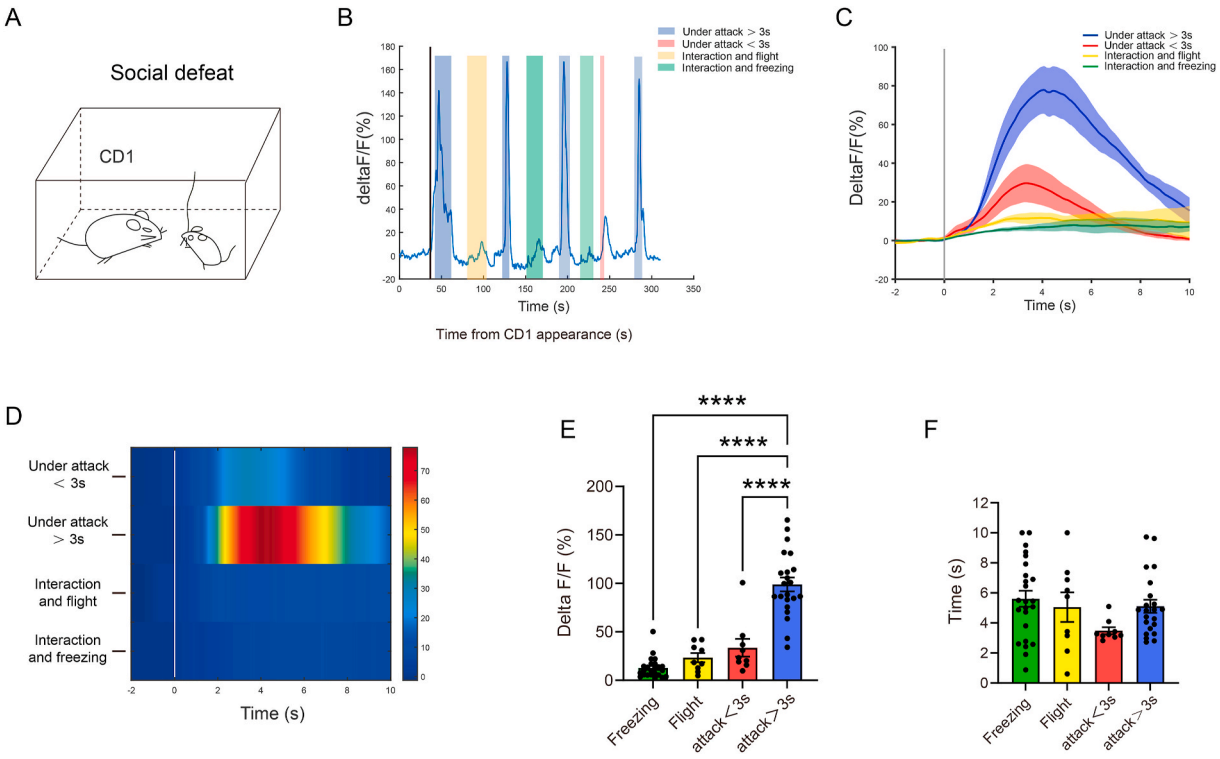

Fig. 6. Changes of astrocytic calcium signaling in the mPFC of mice subjected to social defeat
A. Schematic of social defeat. B. A representative trace showing increases of mPFC astrocytic GCaMP6s signal in recording mice during social contact. Shaded bars depict the periods during which mice are in state of attacked (blue: >3s, pink: <3s), interaction and flight (yellow) or interaction and freezing (green). C. The peri-event plots of the mean Ca^{2+} transient in different states (n = 6 mice). The blue line and the shaded area indicate the mean and SEM in state of under attack >3s, the red line and the shaded area indicate the mean and SEM in state of under attack <3s, the yellow line and the shaded area indicate the mean and SEM in state of interaction and flight and the green line and the shaded area indicate the mean and SEM in state of interaction and freezing. D. Heat map of Ca^{2+} signals aligned to the period during different states of mice (n = 6 mice). E. Comparison of mean peak GCaMP6s signals during different states of mice (respective events from 6 mice). F. Comparison of average time to peak ΔF/F of GCaMP6s signals during different states of mice (respective events from 6 mice).

mPFC astrocyte exhibited the most significant increase in fluorescence intensity (Fig. 6A and C, A: one-way ANOVA, F (1.652, 8.258) = 11.48, P = 0.0052) during EPS tests and the fastest peak arrival time (Fig. 6B and C, B: one-way ANOVA, F (1.792, 8.962) = 12.51, P = 0.003) during FS tests. The changes in calcium signals during TMT exploration were minimal with a prolonged peak latency (Fig. 6A–C). The fluorescence peaks in EPM were comparable to those in TRT or FS (Fig. 6A and C), but the times taken to reach the peak were significantly longer than those in TRT or FS (Fig. 6B and C). In the SD test, the increase in calcium signals elicited by initial attacks in mice resembled the magnitude of the response during TMT exploration (Fig. 6A and C), although the peak latency was shorter than that observed in the TMT test (Fig. 6B and C). Analysis of the mean calcium signal across these six behaviors (three repeated TRTs, three repeated FSs, open arm explorations within 5 min, platform edge explorations during EPS, all TMT explorations and aggression exceeding 3 s) revealed that the mean fluorescence peak of calcium signal was highest during TRT and significantly greater than peaks observed in the EPM, EPS or TMT tests (Fig. 6D and F, D: one-way ANOVA, F (2.737, 13.68) = 13.80, P = 0.0002). The mean peak of calcium signal in the FS test was marginally lower than that in the TRT test, but significantly higher than that in the EPM and TMT tests (Fig. 6D). There was no significant difference in average fluorescence peak values between EPM, EPS, TMT and SD tests (Fig. 6D). The difference in mean latency of peak calcium fluorescence among the six tests mirrored that seen during initial responses (Fig. 6E and F, E: one-way ANOVA, F (2.544, 12.72) = 28.56, P < 0.0001), with shorter latencies were observed during FS and SD while longer latencies occurred during EPM and TMT.

4. Discussion

In this study, we showed that mPFC astrocytes could respond to acute stressful environments and exhibit diverse calcium signaling dynamics. Astrocytic dysfunctions have long been implicated in various neuropsychiatric disorders (Bender et al., 2016; Cotter et al., 2001). For instance, reductions in GFAP positive cells and processes are usually found in hippocampus, prefrontal cortex and amygdala in chronic stressed animals or postmortem tissues of major depression (Bender et al., 2016; Czeh et al., 2006). In acute stressed conditions, such as acute restraint, some studies show that there was no change in GFAP expression (Imbe et al., 2013; Sugama et al., 2011), but many other astrocyte enriched genes, such as s100β (Scaccianoce et al., 2004) and inflammatory protein (Sugama et al., 2011) were changed after acute stress. These studies suggested that astrocyte can sense and change their morphology or functionality in response to stress and may be involved in the development of mood disorders. However, the dynamic changes in astrocyte activity in awake mice under various stress conditions and during behavioral processes are worthy of further exploration.

By using fiber photometry calcium imaging in awake behaving mice, we showed for the first time that mPFC astrocytes respond to diverse stressful environments by elevating calcium signals in a unique manner. The response time and the magnitude of astrocyte calcium signal elevation varied in response to somatosensory, visual, olfactory and social stimuli. We found that unexpected somatic (FS and TRT) and visual (EPS) stimulation induced a faster peak latency of astrocyte calcium signaling, while the expected exploration of stressors (EPM and TMT) had a slightly longer peak latency. In addition, the adaptability of astrocytes to different stressors is also different, which is manifested in the

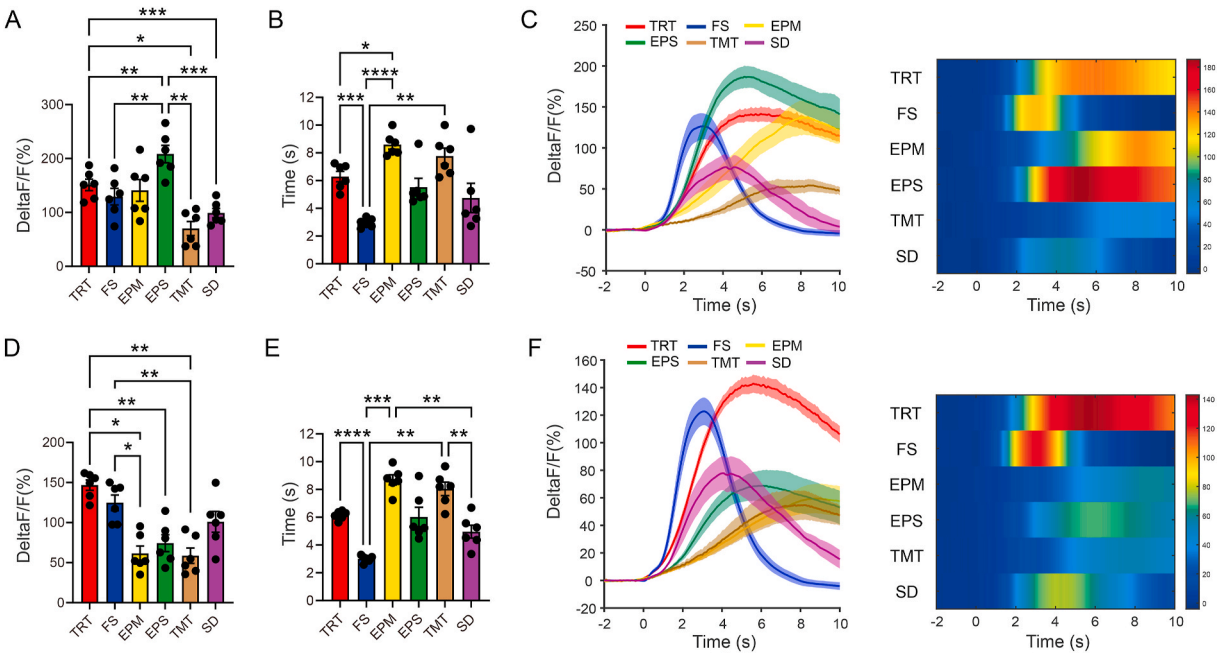

Fig. 7. Calcium dynamics in mPFC astrocytes in response to different aversive stimuli
A. Comparison of average peak ΔF/F of mPFC astrocytic GCaMP6s in response to different aversive stimuli at the first onset of stimulation. B. Comparison of average time to peak ΔF/F of mPFC astrocytic GCaMP6s in response to different aversive stimuli at the first onset of stimulation. C. The peri-event plots and heat map of the mean Ca^{2+} transient in response to different stimuli at the first onset of stimulation. D. Comparison of average peak ΔF/F of mPFC astrocytic GCaMP6s in response to multiple events in different aversive stimuli. E. Comparison of average time to peak ΔF/F of mPFC astrocytic GCaMP6s in response to multiple events in different aversive stimuli. F. The peri-event plots and heat map of the mean Ca^{2+} transient in response to multiple events in different aversive stimuli.

difference in the degree of first and subsequent calcium response to stressors. Our results of astrocyte activity in EPM test are in line with a recent report of hippocampal astrocyte activation observed during the anxiety state in the virtual reality EPM test (Cho et al., 2022). Interestingly, by using two-photon imaging, they identified a cluster of pre-responsive cells (Ca^{2+} increases before entering the center). In our study, the calcium activity of astrocyte populations in the mPFC has a similar response during the exploration of the open arm. However, the sudden stimulation (FS, TRT or EPS) appears to increase both the rate and proportion of pre-responsive cells, consequently leading to a more rapid rise in population calcium activity. Notably, in our odor stimulation test, mPFC astrocytes exhibited increased calcium activity in response to odorless water, neutral, and positive odors. However, the magnitude of this change was much smaller compared to the increase observed during negative odor stimulation. These findings suggest that non-aversive stimuli can also elicit alterations in mPFC astrocytic calcium activity, potentially reflecting changes in mouse attention such as exploratory behavior. Nevertheless, our study demonstrates that different negative stimuli generally evoke stronger and dynamically changing calcium activity in mPFC astrocytes, suggesting that the different responses of mPFC astrocytes can directly reflect the stress state in mice.

There is growing evidence that astrocytes are capable of responding to sensory input and local synaptic transmission. Astrocytes express a variety of neurotransmitter and neuromodulator receptors, including adrenergic receptors, serotonin receptors, etc., and their calcium activity is directly modulated by them (Cahill et al., 2024; Gonzalez-Arias et al., 2023; Reitman et al., 2023). Studies have shown that changes in Ca^{2+} activity in astrocytes correlate with arousal and are sensitive to the release of norepinephrine and acetylcholine (Rasmussen et al., 2023; Reitman et al., 2023). The release of norepinephrine precedes and reaches its peak shortly after the onset of the astrocytic Ca^{2+} signaling in cortical astrocytes (Reitman et al., 2023). The authors propose that astrocytes integrate external sensory signals (synaptic activity) and internal arousal state information (delivered by neuromodulators such as norepinephrine and acetylcholine) via Ca^{2+} signaling. We postulated that distinct sensory stimuli may elicit varying levels of neurotransmitters such as glutamate and norepinephrine release in the mPFC, leading to differential neuronal activation and influencing the arousal state of mice. Astrocytes integrate synaptic information and display diverse calcium activity. Interestingly, SSRIs also activate PFC astrocytes (Schipke et al., 2011), the authors found that the calcium signals induced by stimulation with 5-HT and SSRIs occur time-delayed, asynchronously which is in contrast to glutamate-induced calcium responses in astrocytes. We hypothesize that the rapid changes in astrocytic calcium activity induced by acute stress in our study may firstly reflect alterations in glutamate levels. Prolonged stress results in astrocyte impairment and reduced activity, whereas SSRIs enhance serotonin binding to astrocytes and elevate astrocyte calcium activity.

In our current experiments, the same 6 mice were exposed to all the stress sessions, thus necessitating consideration of the potential impact of previous stresses on the response to further stressors in our study. The limitation of our study lies in the need for further exploration of the mechanisms underlying differential astrocyte activity in response to various types of stress and the role of astrocyte activity in the pathogenesis of neuropsychiatric disorders. In recent years, numerous scholars have documented associations between prefrontal astrocytic activities and depression-like behavior in mice. For instance, targeted removal of PFC astrocytes induces anhedonic behavior, while chemogenetic activates astrocytes reverses chronic restraint stress-induced anhedonia (Codeluppi et al., 2023). Corticosterone-treated mice show reduced astrocytic activities in mPFC, while chronic activation of astrocytes can reduce their immobile time during forced swimming, improve social ability, and exhibit antidepressant effects (Gonzalez-Arias et al., 2023). Modulating the expression of certain genes in mPFC astrocytes can also impact their calcium activity and regulate depression-like behavior in mice (Cao et al., 2013; Guo et al., 2024; Lu et al., 2022; Yao et al., 2023). All of the above studies explored the relationship between changes in astrocyte activity and depression-like behavior under chronic stress conditions. However, our findings

indicated that prefrontal astrocytes were sensitive to multiple acute stressors and showed different activity states. The question that arises is how astrocytes differentiate and process different stressors and thus gradually lose their activity and function during the production of depression-like behaviors. We believed that the change of astrocyte calcium activity may be an adaptive response to the change of internal environment caused by various environmental stimuli. Chronic stimulation above the threshold of astrocyte leads to the disintegration of its activity and the destruction of internal environment, which leads to emotional problems. In future studies, interventions targeting astrocyte calcium activity will be imperative to elucidate the role of negative stimuli in inducing astrocyte response.

In conclusion, our study preliminarily suggests that mPFC astrocytes respond to various negative stimuli in a certain way through differential activity changes, providing a basis for understanding the mechanism of astrocyte inactivation caused by chronic stress and its relationship with depression-like behavior.

Funding

This work was supported by the National Natural Science Foundation of China (No. 81370444, No. 81671316), and Scientific Researching Fund Project of Hefei Second People's Hospital (2022yyb005).

Data availability

The raw data supporting the conclusions of this article will be made available by the authors, without undue reservation.

CRediT authorship contribution statement

Ai-Mei Wu: Writing – original draft, Methodology, Formal analysis, Data curation. **Jing-Ya Zhang:** Data curation. **Wei-Zhong Lun:** Data curation. **Zhi Geng:** Resources. **Ye Yang:** Investigation. **Jun-Cang Wu:** Writing – review & editing, Conceptualization. **Gui-Hai Chen:** Writing – review & editing, Supervision, Funding acquisition, Conceptualization.

Declaration of competing interest

The authors declare that the research was conducted in the absence of any commercial or financial relationships that could be construed as a potential conflict of interest.

Appendix A. Supplementary data

Supplementary data to this article can be found online at https://doi.org/10.1016/j.ynstr.2024.100676.

References

Aten, S., Du, Y., Taylor, O., Dye, C., Collins, K., Thomas, M., Kiyoshi, C., Zhou, M., 2023. Chronic stress impairs the structure and function of astrocyte networks in an animal model of depression. Neurochem. Res. 48 (4), 1191–1210. https://doi.org/10.1007/s11064-022-03663-4.

Barnett, D., Bohmbach, K., Grelot, V., Charlet, A., Dallerac, G., Ju, Y.H., Nagai, J., Orr, A. G., 2023. Astrocytes as drivers and disruptors of behavior: new advances in basic mechanisms and therapeutic targeting. J. Neurosci. 43 (45), 7463–7471. https://doi.org/10.1523/JNEUROSCI.1376-23.2023.

Bazargani, N., Attwell, D., 2016. Astrocyte calcium signaling: the third wave. Nat. Neurosci. 19 (2), 182–189. https://doi.org/10.1038/nn.4201.

Bender, C.L., Calfa, G.D., Molina, V.A., 2016. Astrocyte plasticity induced by emotional stress: a new partner in psychiatric physiopathology? Prog. Neuro-Psychopharmacol. Biol. Psychiatry 65, 68–77. https://doi.org/10.1016/j.pnpbp.2015.08.005.

Cahill, M.K., Collard, M., Tse, V., Reitman, M.E., Etchenique, R., Kirst, C., Poskanzer, K. E., 2024. Network-level encoding of local neurotransmitters in cortical astrocytes. Nature 629 (8010), 146–153. https://doi.org/10.1038/s41586-024-07311-5.

Cao, X., Li, L.P., Wang, Q., Wu, Q., Hu, H.H., Zhang, M., Fang, Y.Y., Zhang, J., Li, S.J., Xiong, W.C., Yan, H.C., Gao, Y.B., Liu, J.H., Li, X.W., Sun, L.R., Zeng, Y.N., Zhu, X.H., Gao, T.M., 2013. Astrocyte-derived ATP modulates depressive-like behaviors. Nat Med 19 (6), 773–777. https://doi.org/10.1038/nm.3162.

Cathomas, F., Holt, L.M., Parise, E.M., Liu, J., Murrough, J.W., Casaccia, P., Nestler, E.J., Russo, S.J., 2022. Beyond the neuron: role of non-neuronal cells in stress disorders. Neuron 110 (7), 1116–1138. https://doi.org/10.1016/j.neuron.2022.01.033.

Cho, W.H., Noh, K., Lee, B.H., Barcelon, E., Jun, S.B., Park, H.Y., Lee, S.J., 2022. Hippocampal astrocytes modulate anxiety-like behavior. Nat. Commun. 13 (1), 6536. https://doi.org/10.1038/s41467-022-34201-z.

Codeluppi, S.A., Xu, M., Bansal, Y., Lepack, A.E., Duric, V., Chow, M., Muir, J., Bagot, R. C., Licznerski, P., Wilber, S.L., Sanacora, G., Sibille, E., Duman, R.S., Pittenger, C., Banasr, M., 2023. Prefrontal cortex astroglia modulate anhedonia-like behavior. Mol Psychiatry 28 (11), 4632–4641. https://doi.org/10.1038/s41380-023-02246-1.

Cotter, D.R., Pariante, C.M., Everall, I.P., 2001. Glial cell abnormalities in major psychiatric disorders: the evidence and implications. Brain Res. Bull. 55 (5), 585–595. https://doi.org/10.1016/s0361-9230(01)00527-5.

Czeh, B., Simon, M., Schmelting, B., Hiemke, C., Fuchs, E., 2006. Astroglial plasticity in the hippocampus is affected by chronic psychosocial stress and concomitant fluoxetine treatment. Neuropsychopharmacology 31 (8), 1616–1626. https://doi.org/10.1038/sj.npp.1300982.

Gonzalez-Arias, C., Sanchez-Ruiz, A., Esparza, J., Sanchez-Puelles, C., Arancibia, L., Ramirez-Franco, J., Gobbo, D., Kirchhoff, F., Perea, G., 2023. Dysfunctional serotonergic neuron-astrocyte signaling in depressive-like states. Mol Psychiatry 28 (9), 3856–3873. https://doi.org/10.1038/s41380-023-02269-8.

Guo, F., Fan, J., Liu, J.M., Kong, P.L., Ren, J., Mo, J.W., Lu, C.L., Zhong, Q.L., Chen, L.Y., Jiang, H.T., Zhang, C., Wen, Y.L., Gu, T.T., Li, S.J., Fang, Y.Y., Pan, B.X., Gao, T.M., Cao, X., 2024. Astrocytic ALKBH5 in stress response contributes to depressive-like behaviors in mice. Nat. Commun. 15 (1), 4347. https://doi.org/10.1038/s41467-024-48730-2.

Imbe, H., Kimura, A., Donishi, T., Kaneoke, Y., 2013. Effects of restraint stress on glial activity in the rostral ventromedial medulla. Neuroscience 241, 10–21. https://doi.org/10.1016/j.neuroscience.2013.03.008.

Kim, J., Lee, S., Fang, Y.Y., Shin, A., Park, S., Hashikawa, K., Bhat, S., Kim, D., Sohn, J. W., Lin, D., Suh, G.S.B., 2019. Rapid, biphasic CRF neuronal responses encode positive and negative valence. Nat. Neurosci. 22 (4), 576–585. https://doi.org/10.1038/s41593-019-0342-2.

Kofuji, P., Araque, A., 2021. Astrocytes and behavior. Annu. Rev. Neurosci. 44, 49–67. https://doi.org/10.1146/annurev-neuro-101920-112225.

Lu, C.L., Ren, J., Mo, J.W., Fan, J., Guo, F., Chen, L.Y., Wen, Y.L., Li, S.J., Fang, Y.Y., Wu, Z.F., Li, Y.L., Gao, T.M., Cao, X., 2022. Glucocorticoid receptor-dependent astrocytes mediate stress vulnerability. Biol Psychiatry 92 (3), 204–215. https://doi.org/10.1016/j.biopsych.2021.11.022.

Murphy-Royal, C., Gordon, G.R., Bains, J.S., 2019. Stress-induced structural and functional modifications of astrocytes-Further implicating glia in the central response to stress. Glia 67 (10), 1806–1820. https://doi.org/10.1002/glia.23610.

Nagai, J., Yu, X., Papouin, T., Cheong, E., Freeman, M.R., Monk, K.R., Hastings, M.H., Haydon, P.G., Rowitch, D., Shaham, S., Khakh, B.S., 2021. Behaviorally consequential astrocytic regulation of neural circuits. Neuron 109 (4), 576–596. https://doi.org/10.1016/j.neuron.2020.12.008.

Noh, K., Cho, W.H., Lee, B.H., Kim, D.W., Kim, Y.S., Park, K., Hwang, M., Barcelon, E., Cho, Y.K., Lee, C.J., Yoon, B.E., Choi, S.Y., Park, H.Y., Jun, S.B., Lee, S.J., 2023. Cortical astrocytes modulate dominance behavior in male mice by regulating synaptic excitatory and inhibitory balance. Nat. Neurosci. 26 (9), 1541–1554. https://doi.org/10.1038/s41593-023-01406-4.

Rasmussen, R.N., Asiminas, A., Carlsen, E.M.M., Kjaerby, C., Smith, N.A., 2023. Astrocytes: integrators of arousal state and sensory context. Trends Neurosci. 46 (6), 418–425. https://doi.org/10.1016/j.tins.2023.03.003.

Reitman, M.E., Tse, V., Mi, X., Willoughby, D.D., Peinado, A., Aivazidis, A., Myagmar, B. E., Simpson, P.C., Bayraktar, O.A., Yu, G., Poskanzer, K.E., 2023. Norepinephrine links astrocytic activity to regulation of cortical state. Nat. Neurosci. 26 (4), 579–593. https://doi.org/10.1038/s41593-023-01284-w.

Saraiva, L.R., Kondoh, K., Ye, X., Yoon, K.H., Hernandez, M., Buck, L.B., 2016. Combinatorial effects of odorants on mouse behavior. Proc Natl Acad Sci U S A 113 (23), E3300–E3306. https://doi.org/10.1073/pnas.1605973113.

Scaccianoce, S., Del Bianco, P., Pannitteri, G., Passarelli, F., 2004. Relationship between stress and circulating levels of S100B protein. Brain Res. 1004 (1–2), 208–211. https://doi.org/10.1016/j.brainres.2004.01.028.

Schipke, C.G., Heuser, I., Peters, O., 2011. Antidepressants act on glial cells: SSRIs and serotonin elicit astrocyte calcium signaling in the mouse prefrontal cortex. J. Psychiatr. Res. 45 (2), 242–248. https://doi.org/10.1016/j.jpsychires.2010.06.005.

Semyanov, A., Henneberger, C., Agarwal, A., 2020. Making sense of astrocytic calcium signals - from acquisition to interpretation. Nat. Rev. Neurosci. 21 (10), 551–564. https://doi.org/10.1038/s41583-020-0361-8.

Sofroniew, M.V., Vinters, H.V., 2010. Astrocytes: biology and pathology. Acta Neuropathol. 119 (1), 7–35. https://doi.org/10.1007/s00401-009-0619-8.

Sugama, S., Takenouchi, T., Sekiyama, K., Kitani, H., Hashimoto, M., 2011. Immunological responses of astroglia in the rat brain under acute stress: interleukin 1 beta co-localized in astroglia. Neuroscience 192, 429–437. https://doi.org/10.1016/j.neuroscience.2011.06.051.

Volterra, A., Meldolesi, J., 2005. Astrocytes, from brain glue to communication elements: the revolution continues. Nat. Rev. Neurosci. 6 (8), 626–640. https://doi.org/10.1038/nrn1722.

Wang, J., Yang, Q., Liu, X., Li, J., Wen, Y.L., Hu, Y., Xu, T.L., Duan, S., Xu, H., 2024. The basal forebrain to lateral habenula circuitry mediates social behavioral maladaptation. Nat. Commun. 15 (1), 4013. https://doi.org/10.1038/s41467-024-48378-y.

Yan, C., Liu, Z., 2024. The role of periaqueductal gray astrocytes in anxiety-like behavior induced by acute stress. Biochem. Biophys. Res. Commun. 720, 150073. https://doi.org/10.1016/j.bbrc.2024.150073.

Yao, S., Xu, M.D., Wang, Y., Zhao, S.T., Wang, J., Chen, G.F., Chen, W.B., Liu, J., Huang, G.B., Sun, W.J., Zhang, Y.Y., Hou, H.L., Li, L., Sun, X.D., 2023. Astrocytic lactate dehydrogenase A regulates neuronal excitability and depressive-like behaviors through lactate homeostasis in mice. Nat. Commun. 14 (1), 729. https://doi.org/10.1038/s41467-023-36209-5.

Zhang, X., Lei, B., Yuan, Y., Zhang, L., Hu, L., Jin, S., Kang, B., Liao, X., Sun, W., Xu, F., Zhong, Y., Hu, J., Qi, H., 2020. Brain control of humoral immune responses amenable to behavioural modulation. Nature 581 (7807), 204–208. https://doi.org/10.1038/s41586-020-2235-7.

Zhou, X., Xiao, Q., Liu, Y., Chen, S., Xu, X., Zhang, Z., Hong, Y., Shao, J., Chen, Y., Chen, Y., Wang, L., Yang, F., Tu, J., 2024. Astrocyte-mediated regulation of BLA (WFS1) neurons alleviates risk-assessment deficits in DISC1-N mice. Neuron. https://doi.org/10.1016/j.neuron.2024.03.028.